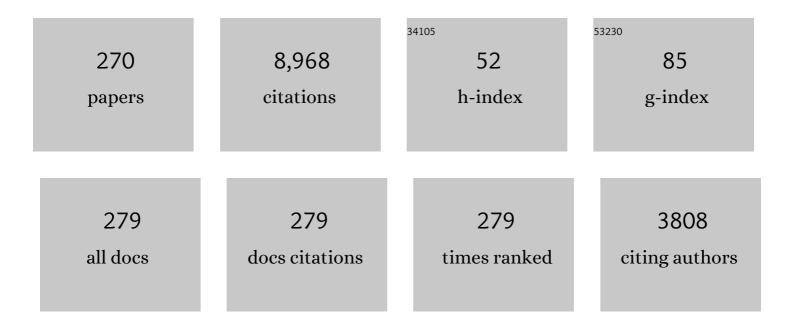
List of Publications by Year in descending order

Source: https://exaly.com/author-pdf/7836448/publications.pdf Version: 2024-02-01



MAXIM LEREDEV

#	Article	IF	CITATIONS
1	Seismic wave attenuation and dispersion resulting from wave-induced flow in porous rocks — A review. Geophysics, 2010, 75, 75A147-75A164.	2.6	704
2	Wettability alteration of oil-wet carbonate by silica nanofluid. Journal of Colloid and Interface Science, 2016, 461, 435-442.	9.4	332
3	Microstructure and Electrical Properties of Lead Zirconate Titanate (Pb(Zr52/Ti48)O3) Thick Films Deposited by Aerosol Deposition Method. Japanese Journal of Applied Physics, 1999, 38, 5397-5401.	1.5	313
4	Piezoelectric properties and poling effect of Pb(Zr, Ti)O3 thick films prepared for microactuators by aerosol deposition. Applied Physics Letters, 2000, 77, 1710-1712.	3.3	208
5	CO ₂ wettability of caprocks: Implications for structural storage capacity and containment security. Geophysical Research Letters, 2015, 42, 9279-9284.	4.0	192
6	Impact of pressure and temperature on CO 2 –brine–mica contact angles and CO 2 –brine interfacial tension: Implications for carbon geo-sequestration. Journal of Colloid and Interface Science, 2016, 462, 208-215.	9.4	190
7	Receding and advancing (CO 2 + brine + quartz) contact angles as a function of pressure, temperature, surface roughness, salt type and salinity. Journal of Chemical Thermodynamics, 2016, 93, 416-423.	2.0	174
8	Wettability of rock/CO2/brine and rock/oil/CO2-enriched-brine systems:Critical parametric analysis and future outlook. Advances in Colloid and Interface Science, 2019, 268, 91-113.	14.7	138
9	Multi-scale x-ray computed tomography analysis of coal microstructure and permeability changes as a function of effective stress. International Journal of Coal Geology, 2016, 165, 149-156.	5.0	130
10	Residual trapping of supercritical CO2 in oil-wet sandstone. Journal of Colloid and Interface Science, 2016, 469, 63-68.	9.4	124
11	Influence of Carrier Gas Conditions on Electrical and Optical Properties of Pb(Zr, Ti)O3Thin Films Prepared by Aerosol Deposition Method. Japanese Journal of Applied Physics, 2001, 40, 5528-5532.	1.5	116
12	Wettability of nanofluid-modified oil-wet calcite at reservoir conditions. Fuel, 2018, 211, 405-414.	6.4	116
13	Effect of temperature and SiO2 nanoparticle size on wettability alteration of oil-wet calcite. Fuel, 2017, 206, 34-42.	6.4	115
14	Swellingâ€induced changes in coal microstructure due to supercritical CO ₂ injection. Geophysical Research Letters, 2016, 43, 9077-9083.	4.0	111
15	CO2 storage in carbonates: Wettability of calcite. International Journal of Greenhouse Gas Control, 2017, 62, 113-121.	4.6	108
16	Carbon geosequestration in limestone: Pore-scale dissolution and geomechanical weakening. International Journal of Greenhouse Gas Control, 2017, 66, 106-119.	4.6	108
17	Influence of shaleâ€ŧotal organic content on CO ₂ geoâ€storage potential. Geophysical Research Letters, 2017, 44, 8769-8775.	4.0	107
18	Wettability alteration of oil-wet limestone using surfactant-nanoparticle formulation. Journal of Colloid and Interface Science, 2017, 504, 334-345.	9.4	106

#	Article	IF	CITATIONS
19	Solid/CO 2 and solid/water interfacial tensions as a function of pressure, temperature, salinity and mineral type: Implications for CO 2 -wettability and CO 2 geo-storage. International Journal of Greenhouse Gas Control, 2016, 53, 263-273.	4.6	103
20	Pore-scale analysis of coal cleat network evolution through liquid nitrogen treatment: A Micro-Computed Tomography investigation. International Journal of Coal Geology, 2020, 219, 103370.	5.0	99
21	Swelling effect on coal micro structure and associated permeability reduction. Fuel, 2016, 182, 568-576.	6.4	97
22	Powder Preparation in Aerosol Deposition Method for Lead Zirconate Titanate Thick Films. Japanese Journal of Applied Physics, 2002, 41, 6980-6984.	1.5	91
23	Organic acid concentration thresholds for ageing of carbonate minerals: Implications for CO2 trapping/storage. Journal of Colloid and Interface Science, 2019, 534, 88-94.	9.4	91
24	CO2-wettability of low to high rank coal seams: Implications for carbon sequestration and enhanced methane recovery. Fuel, 2016, 181, 680-689.	6.4	89
25	Wettability Alteration of Quartz Surface by Low-Salinity Surfactant Nanofluids at High-Pressure and High-Temperature Conditions. Energy & Fuels, 2019, 33, 7062-7068.	5.1	89
26	Dependence of quartz wettability on fluid density. Geophysical Research Letters, 2016, 43, 3771-3776.	4.0	88
27	Stabilising nanofluids in saline environments. Journal of Colloid and Interface Science, 2017, 508, 222-229.	9.4	88
28	CO2-wettability of sandstones exposed to traces of organic acids: Implications for CO2 geo-storage. International Journal of Greenhouse Gas Control, 2019, 83, 61-68.	4.6	88
29	Nanoscale rock mechanical property changes in heterogeneous coal after water adsorption. Fuel, 2018, 218, 23-32.	6.4	85
30	Structural trapping capacity of oil-wet caprock as a function of pressure, temperature and salinity. International Journal of Greenhouse Gas Control, 2016, 50, 112-120.	4.6	84
31	Direct laboratory observation of patchy saturation and its effects on ultrasonic velocities. The Leading Edge, 2009, 28, 24-27.	0.7	83
32	Pore-scale analysis of formation damage in Bentheimer sandstone with in-situ NMR and micro-computed tomography experiments. Journal of Petroleum Science and Engineering, 2015, 129, 48-57.	4.2	79
33	Experimental determination of hydrate phase equilibrium for different gas mixtures containing methane, carbon dioxide and nitrogen with motor current measurements. Journal of Natural Gas Science and Engineering, 2017, 38, 59-73.	4.4	79
34	Pore scale investigation of low salinity surfactant nanofluid injection into oil saturated sandstone via X-ray micro-tomography. Journal of Colloid and Interface Science, 2020, 562, 370-380.	9.4	78
35	Nanoparticles influence on wetting behaviour of fractured limestone formation. Journal of Petroleum Science and Engineering, 2017, 149, 782-788.	4.2	77
36	Micro-scale fracturing mechanisms in coal induced by adsorption of supercritical CO 2. International Journal of Coal Geology, 2017, 175, 40-50.	5.0	76

#	Article	IF	CITATIONS
37	A new method for TOC estimation in tight shale gas reservoirs. International Journal of Coal Geology, 2017, 179, 269-277.	5.0	76
38	Shale Wettability: Data Sets, Challenges, and Outlook. Energy & Fuels, 2021, 35, 2965-2980.	5.1	76
39	Actuation Properties of Lead Zirconate Titanate Thick Films Structured on Si Membrane by the Aerosol Deposition Method. Japanese Journal of Applied Physics, 2000, 39, 5600-5603.	1.5	72
40	X-ray tomography imaging of shale microstructures: A review in the context of multiscale correlative imaging. International Journal of Coal Geology, 2021, 233, 103641.	5.0	69
41	Simple self-selective method of velocity measurement for particles in impact-based deposition. Journal of Vacuum Science and Technology A: Vacuum, Surfaces and Films, 2000, 18, 563-566.	2.1	67
42	Effect of CT image size and resolution on the accuracy of rock property estimates. Journal of Geophysical Research: Solid Earth, 2017, 122, 3635-3647.	3.4	65
43	Effects of annealing and poling conditions on piezoelectric properties of Pb(Zr0.52,Ti0.48)O3 thick films formed by aerosol deposition method. Journal of Crystal Growth, 2002, 235, 415-420.	1.5	63
44	Influence of surface chemistry on interfacial properties of low to high rank coal seams. Fuel, 2017, 194, 211-221.	6.4	63
45	Effect of humic acid on CO2-wettability in sandstone formation. Journal of Colloid and Interface Science, 2021, 588, 315-325.	9.4	63
46	Carbon Dioxide/Brine, Nitrogen/Brine, and Oil/Brine Wettability of Montmorillonite, Illite, and Kaolinite at Elevated Pressure and Temperature. Energy & Fuels, 2019, 33, 441-448.	5.1	61
47	High-Speed Optical Microscanner Driven with Resonation of Lam Waves Using Pb(Zr,Ti)O3Thick Films Formed by Aerosol Deposition. Japanese Journal of Applied Physics, 2005, 44, 7072-7077.	1.5	60
48	N2+CO2+NaCl brine interfacial tensions and contact angles on quartz at CO2 storage site conditions in the Gippsland basin, Victoria/Australia. Journal of Petroleum Science and Engineering, 2015, 129, 58-62.	4.2	60
49	A laboratory study of low-frequency wave dispersion and attenuation in water-saturated sandstones. The Leading Edge, 2014, 33, 616-622.	0.7	58
50	Permeability Evolution in Sandstone Due to CO ₂ Injection. Energy & Fuels, 2017, 31, 12390-12398.	5.1	55
51	Residual Trapping of CO ₂ in an Oilâ€Filled, Oilâ€Wet Sandstone Core: Results of Threeâ€Phase Pore‣cale Imaging. Geophysical Research Letters, 2019, 46, 11146-11154.	4.0	53
52	Influence of Wettability on Residual Gas Trapping and Enhanced Oil Recovery in Three-Phase Flow: A Pore-Scale Analysis by Use of Microcomputed Tomography. SPE Journal, 2016, 21, 1916-1929.	3.1	52
53	Effect of the Temperature on CO ₂ /Brine/Dolomite Wettability: Hydrophilic versus Hydrophobic Surfaces. Energy & Fuels, 2017, 31, 6329-6333.	5.1	52
54	High pressure-elevated temperature x-ray micro-computed tomography for subsurface applications. Advances in Colloid and Interface Science, 2018, 256, 393-410.	14.7	52

#	Article	IF	CITATIONS
55	Pore scale investigation of hydrogen injection in sandstone via X-ray micro-tomography. International Journal of Hydrogen Energy, 2021, 46, 34822-34829.	7.1	52
56	Liquid nitrogen fracturing efficiency as a function of coal rank: A multi-scale tomographic study. Journal of Natural Gas Science and Engineering, 2021, 95, 104177.	4.4	52
57	Wettability of nano-treated calcite/CO 2 /brine systems: Implication for enhanced CO 2 storage potential. International Journal of Greenhouse Gas Control, 2017, 66, 97-105.	4.6	50
58	Carbon dioxide/brine wettability of porous sandstone versus solid quartz: An experimental and theoretical investigation. Journal of Colloid and Interface Science, 2018, 524, 188-194.	9.4	49
59	Simulation and experimental measurements of internal magnetic field gradients and NMR transverse relaxation times (T2) in sandstone rocks. Journal of Petroleum Science and Engineering, 2019, 175, 985-997.	4.2	49
60	Experimental investigation of carbonate wettability as a function of mineralogical and thermo-physical conditions. Fuel, 2020, 264, 116846.	6.4	49
61	Analysis of highâ€resolution Xâ€ray computed tomography images of Bentheim sandstone under elevated confining pressures. Geophysical Prospecting, 2016, 64, 848-859.	1.9	48
62	Electrochemical investigation of the effect of temperature, salinity and salt type on brine/mineral interfacial properties. International Journal of Greenhouse Gas Control, 2017, 59, 136-147.	4.6	48
63	Quantifying the effect of capillarity on attenuation and dispersion in patchy-saturated rocks. Geophysics, 2014, 79, WB35-WB50.	2.6	47
64	Experimental pore-scale analysis of carbon dioxide hydrate in sandstone via X-Ray micro-computed tomography. International Journal of Greenhouse Gas Control, 2018, 79, 73-82.	4.6	47
65	Hydrogen storage potential of coals as a function of pressure, temperature, and rank. Journal of Colloid and Interface Science, 2022, 620, 86-93.	9.4	47
66	A novel hybrid method for gas hydrate filling modes identification via digital rock. Marine and Petroleum Geology, 2020, 115, 104255.	3.3	46
67	An experimental study of solid matrix weakening in waterâ€saturated Savonnières limestone. Geophysical Prospecting, 2014, 62, 1253-1265.	1.9	45
68	Magnetic properties of Sm-Fe-N thick film magnets prepared by the aerosol deposition method. IEEE Transactions on Magnetics, 2003, 39, 2986-2988.	2.1	44
69	Computational elastic upâ€scaling of sandstone on the basis of Xâ€ray microâ€ŧomographic images. Geophysical Prospecting, 2013, 61, 287-301.	1.9	44
70	Microstructural Effects on Mechanical Properties of Shaly Sandstone. Journal of Geotechnical and Geoenvironmental Engineering - ASCE, 2018, 144, .	3.0	43
71	In-situ X-ray micro-computed tomography imaging of the microstructural changes in water-bearing medium rank coal by supercritical CO2 flooding. International Journal of Coal Geology, 2019, 203, 28-35.	5.0	43
72	Characterization of nanoscale rockmechanical properties and microstructures of a Chinese sub-bituminous coal. Journal of Natural Gas Science and Engineering, 2018, 52, 106-116.	4.4	42

#	Article	IF	CITATIONS
73	Experimental estimation of velocities and anisotropy of a series of Swedish crystalline rocks and ores. Geophysical Prospecting, 2013, 61, 153-167.	1.9	41
74	An experimental study of acoustic responses on the injection of supercritical CO2 into sandstones from the Otway Basin. Geophysics, 2013, 78, D293-D306.	2.6	40
75	Validation of the laboratory measurements at seismic frequencies using the Kramersâ€Kronig relationship. Geophysical Research Letters, 2016, 43, 4986-4991.	4.0	40
76	Nanoscale geomechanical properties of Western Australian coal. Journal of Petroleum Science and Engineering, 2018, 162, 736-746.	4.2	40
77	Laboratory measurements of the effect of fluid saturation on elastic properties of carbonates at seismic frequencies. Geophysical Prospecting, 2016, 64, 799-809.	1.9	39
78	CO 2 geo-storage capacity enhancement via nanofluid priming. International Journal of Greenhouse Gas Control, 2017, 63, 20-25.	4.6	39
79	Porosity estimation in kerogen-bearing shale gas reservoirs. Journal of Natural Gas Science and Engineering, 2018, 52, 575-581.	4.4	37
80	Substrate heating effects on hardness of an -Al2O3 thick film formed by aerosol deposition method. Journal of Crystal Growth, 2005, 275, e1301-e1306.	1.5	36
81	Compressional wave velocity of hydrate-bearing bentheimer sediments with varying pore fillings. International Journal of Hydrogen Energy, 2018, 43, 23193-23200.	7.1	36
82	Geochemical controls on wettability alteration at pore-scale during low salinity water flooding in sandstone using X-ray micro computed tomography. Fuel, 2020, 271, 117675.	6.4	36
83	Micro-Cleat and Permeability Evolution of Anisotropic Coal During Directional CO2 Flooding: An In Situ Micro-CT Study. Natural Resources Research, 2022, 31, 2805-2818.	4.7	36
84	Effect of Thickness on the Piezoelectric Properties of Lead Zirconate Titanate Films Fabricated by Aerosol Deposition Method. Japanese Journal of Applied Physics, 2002, 41, 6669-6673.	1.5	35
85	Hydrogen Flooding of a Coal Core: Effect on Coal Swelling. Geophysical Research Letters, 2022, 49, .	4.0	35
86	Measurements of the elastic and anelastic properties of sandstone flooded with supercritical CO ₂ . Geophysical Prospecting, 2014, 62, 1266-1277.	1.9	33
87	Wave-velocity dispersion and rock microstructure. Journal of Petroleum Science and Engineering, 2019, 183, 106466.	4.2	31
88	Influence of pore structural properties on gas hydrate saturation and permeability: A coupled pore-scale modelling and X-ray computed tomography method. Journal of Natural Gas Science and Engineering, 2021, 88, 103805.	4.4	31
89	Cubic Aluminum Nitride Transformed Under Reduced Pressure Using Aerosol Deposition Method. Journal of the American Ceramic Society, 2005, 88, 1067-1069.	3.8	30
90	Digital carbonate rock physics. Solid Earth, 2016, 7, 1185-1197.	2.8	30

#	Article	IF	CITATIONS
91	Fluid–rock interactions and its implications on EOR: Critical analysis, experimental techniques and knowledge gaps. Energy Reports, 2022, 8, 6355-6395.	5.1	30
92	Initial and residual trapping of hydrogen and nitrogen in Fontainebleau sandstone using nuclear magnetic resonance core flooding. International Journal of Hydrogen Energy, 2022, 47, 22482-22494.	7.1	30
93	Permeability evolution in sandstone due to injection of CO2-saturated brine or supercritical CO2 at reservoir conditions. Energy Procedia, 2014, 63, 3051-3059.	1.8	29
94	Sorptionâ€Induced Deformation and Elastic Weakening of Bentheim Sandstone. Journal of Geophysical Research: Solid Earth, 2018, 123, 8589-8601.	3.4	29
95	Forced imbibition into a limestone: measuring Pâ€wave velocity and water saturation dependence on injection rate. Geophysical Prospecting, 2014, 62, 1126-1142.	1.9	28
96	Impact of fines and rock wettability on reservoir formation damage. Geophysical Prospecting, 2016, 64, 860-874.	1.9	28
97	Coal Wettability After CO ₂ Injection. Energy & Fuels, 2017, 31, 12376-12382.	5.1	27
98	Interaction of low salinity surfactant nanofluids with carbonate surfaces and molecular level dynamics at fluid-fluid interface at ScCO2 loading. Journal of Colloid and Interface Science, 2021, 586, 315-325.	9.4	27
99	Neutron scattering: A subsurface application review. Earth-Science Reviews, 2021, 221, 103755.	9.1	26
100	Coal fracturing through liquid nitrogen treatment: a micro-computed tomography study. APPEA Journal, 2020, 60, 67.	0.2	25
101	Feasibility of CO ₂ plume detection using 4D seismic: CO2CRC Otway Project case study — Part 1: Rock-physics modeling. Geophysics, 2015, 80, B95-B104.	2.6	24
102	Coal cleat network evolution through liquid nitrogen freeze-thaw cycling. Fuel, 2022, 314, 123069.	6.4	24
103	What Thickness of the Piezoelectric Layer with High Breakdown Voltage is Required for the Microactuator?. Japanese Journal of Applied Physics, 2002, 41, 3344-3347.	1.5	23
104	Title is missing!. Materia Japan, 2002, 41, 459-466.	0.1	23
105	Elastic anisotropy estimation from laboratory measurements of velocity and polarization of quasi-P-waves using laser interferometry. Geophysics, 2011, 76, WA83-WA89.	2.6	23
106	Compaction of quartz-kaolinite mixtures: The influence of the pore fluid composition on the development of their microstructure and elastic anisotropy. Marine and Petroleum Geology, 2016, 78, 426-438.	3.3	23
107	X-ray micro-computed tomography and ultrasonic velocity analysis of fractured shale as a function of effective stress. Marine and Petroleum Geology, 2019, 110, 472-482.	3.3	23
108	Residual Trapping of Supercritical CO2: Direct Pore-scale Observation Using a Low Cost Pressure Cell for Micro Computer Tomography. Energy Procedia, 2017, 114, 4967-4974.	1.8	22

#	Article	IF	CITATIONS
109	Coal fines migration: A holistic review of influencing factors. Advances in Colloid and Interface Science, 2022, 301, 102595.	14.7	22
110	Electro-Optical Properties of (Pb, La)(Zr, Ti)O3Films Prepared by Aerosol Deposition Method. Japanese Journal of Applied Physics, 2003, 42, 5960-5962.	1.5	21
111	Theoretical and Experimental Investigation of Propagation of Guide Waves in Cylindrical Pipe Filled with Fluid. Japanese Journal of Applied Physics, 2006, 45, 4573-4576.	1.5	21
112	Optically transparent, dense \hat{I}_\pm -Al2O3 thick films deposited on glass at room temperature. Current Applied Physics, 2008, 8, 233-236.	2.4	21
113	Effect of asperities on stress dependency of elastic properties of cracked rocks. International Journal of Engineering Science, 2016, 98, 116-125.	5.0	21
114	Morphological evaluation of heterogeneous oolitic limestone under pressure and fluid flow using X-ray microtomography. Journal of Applied Geophysics, 2018, 150, 172-181.	2.1	21
115	Carbonate rock mechanical response to CO2 flooding evaluated by a combined X-ray computed tomography – DEM method. Journal of Natural Gas Science and Engineering, 2020, 84, 103675.	4.4	21
116	NiZnCu Ferrite Thick Film with Nano Scale Crystallites Formed by the Aerosol Deposition Method. Journal of the American Ceramic Society, 2004, 87, 1621-1624.	3.8	20
117	Influence of Miscible CO2 Flooding on Wettability and Asphaltene Precipitation in Indiana Lime Stone. , 2017, , .		20
118	Aerosol Deposition Method for Preparation of Lead Zirconate Titanate Thick Layer at Low Temperature –Improvement of Electrical Properties by Irradiation of Fast Atom Beam and Plasma–. Japanese Journal of Applied Physics, 2003, 42, 5931-5935.	1.5	19
119	A Laboratory Study of the Elastic and Anelastic Properties of the Sandstone Flooded with Supercritical CO2 at Seismic Frequencies. Energy Procedia, 2014, 63, 4289-4296.	1.8	19
120	Influence of gas hydrate saturation and pore habits on gas relative permeability in gas hydrate-bearing sediments: Theory, experiment and case study. Journal of Natural Gas Science and Engineering, 2021, 95, 104171.	4.4	19
121	Effect of supercritical CO ₂ on carbonates: Savonnières sample case study. Geophysical Prospecting, 2017, 65, 251-265.	1.9	18
122	Water retention effects on elastic properties of Opalinus shale. Geophysical Prospecting, 2019, 67, 984-996.	1.9	18
123	A laboratory study of attenuation and dispersion effects in glycerol-saturated Berea sandstone at seismic frequencies. , 2015, , .		17
124	Impact of Solid Surface Energy on Wettability of CO2-brine-Mineral Systems as a Function of Pressure, Temperature and Salinity. Energy Procedia, 2017, 114, 4832-4842.	1.8	17
125	Wettability Alteration of Carbonate Rocks via Nanoparticle-Anionic Surfactant Flooding at Reservoirs Conditions. , 2017, , .		17
126	Ultrasonic velocity measurements on thin rock samples: Experiment and numerical modeling. Geophysics, 2018, 83, MR47-MR56.	2.6	17

#	Article	IF	CITATIONS
127	Nano-mechanical Properties and Pore-Scale Characterization of Different Rank Coals. Natural Resources Research, 2020, 29, 1787-1800.	4.7	17
128	Low Salinity Surfactant Nanofluids For Enhanced CO2 Storage Application At High Pressure And Temperature. , 2018, , .		16
129	Geo-Mechanical Weakening of Limestone Due to Supercritical CO2 Injection. , 2016, , .		15
130	A lowâ€frequency laboratory apparatus for measuring elastic and anelastic properties of rocks. , 2011, , .		14
131	Compaction trends of full stiffness tensor and fluid permeability in artificial shales. Geophysical Journal International, 2018, 212, 1687-1693.	2.4	14
132	Simulating Coal Permeability Change as a Function of Effective Stress Using a Microscale Digital Rock Model. Energy & Fuels, 2021, 35, 8756-8762.	5.1	14
133	Patterning Properties of PZT Thick Films Made by Aerosol Deposition. Ferroelectrics, 2002, 270, 117-122.	0.6	13
134	Theoretical Investigation of Guide Wave Flowmeter. Japanese Journal of Applied Physics, 2007, 46, 4521.	1.5	12
135	Research note: Laboratory study of the influence of changing the injection rate on the geometry of the fluid front and on Pâ€wave ultrasonic velocities in sandstone. Geophysical Prospecting, 2012, 60, 572-580.	1.9	12
136	Seismic dispersion and attenuation in Mancos shale – laboratory measurements. Geophysical Prospecting, 2021, 69, 568-585.	1.9	12
137	The rock mechanical properties of lacustrine shales: Argillaceous shales versus silty laminae shales. Marine and Petroleum Geology, 2022, 141, 105707.	3.3	12
138	Aerosol Deposition Method (Adm) For Nano-Crystal Ceramics Coating Without Firing. Materials Research Society Symposia Proceedings, 2003, 778, 8101/W7.10.1.	0.1	11
139	Change in Geomechanical Properties of Limestone Due to Supercritical CO2 Injection. , 2016, , .		11
140	Magnetic properties and microstructures of the aerosol-deposited permanent magnet films. Journal of Magnetism and Magnetic Materials, 2004, 272-276, E1881-E1882.	2.3	10
141	Influence of Rock Microstructure on its Electrical Properties: An Analysis Using X-ray Microcomputed Tomography. Energy Procedia, 2017, 114, 5023-5031.	1.8	10
142	Research note: the effect of strain amplitude produced by ultrasonic waves on its velocity. Geophysical Prospecting, 2019, 67, 715-722.	1.9	10
143	CO 2 â€Saturated Brine Injection Into Unconsolidated Sandstone: Implications for Carbon Geosequestration. Journal of Geophysical Research: Solid Earth, 2019, 124, 10823-10838.	3.4	10
144	Electrical formation factor of clean sand from laboratory measurements and digital rock physics. Solid Earth, 2019, 10, 1505-1517.	2.8	10

#	Article	IF	CITATIONS
145	Experimental study of temperature change effect on distributed acoustic sensing continuous measurements. Geophysics, 2022, 87, D111-D122.	2.6	10
146	Growth rate, microstructure and conformality as a function of vapor exposure for zirconia thin films by pulsed-pressure MOCVD. Surface and Coatings Technology, 2007, 201, 8908-8913.	4.8	9
147	Acoustic Response of Reservoir Sandstones during Injection of Supercritical CO2. Energy Procedia, 2014, 63, 4281-4288.	1.8	9
148	CO2 Wettability of Shales and Coals as a Function of Pressure, Temperature and Rank: Implications for CO2 Sequestration and Enhanced Methane Recovery. , 2016, , .		9
149	A triple porosity scheme for fluid/solid substitution: theory and experiment. Geophysical Prospecting, 2019, 67, 888-899.	1.9	9
150	Rock/Fluid/Polymer Interaction Mechanisms: Implications for Water Shut-off Treatment. Energy & Fuels, 2021, 35, 12809-12827.	5.1	9
151	Experimental Laboratory Study on the Acoustic Response of Sandstones During Injection of Supercritical CO2 on CRC2 Sample from Otway Basin Australia. Energy Procedia, 2013, 37, 4106-4113.	1.8	8
152	Velocityâ€saturation relation in partially saturated rocks: Modelling the effect of injection rate changes. Geophysical Prospecting, 2016, 64, 1054-1066.	1.9	8
153	Modeling of Compaction Trends of Anisotropic Elastic Properties of Shales. Journal of Geophysical Research: Solid Earth, 2021, 126, .	3.4	8
154	Integral effects of initial fluids configuration and wettability alteration on remaining saturation: characterization with X-ray micro-computed tomography. Fuel, 2021, 306, 121717.	6.4	8
155	Coal microstructure changes due to water absorption and CO2 injection. APPEA Journal, 2016, 56, 593.	0.2	8
156	Aerosol Deposition Method (ADM) for Nano-Crystal Ceramics Coating Without Firing. Materials Research Society Symposia Proceedings, 2003, 779, 7101.	0.1	7
157	Precursor system for bio-integration ceramics and deposition onto tantala scaffold bone interface surfaces. Surface and Coatings Technology, 2007, 201, 9413-9416.	4.8	7
158	The CO2CRC Otway shallow CO2 controlled release experiment: Preparation for Phase 2. Energy Procedia, 2018, 154, 145-150.	1.8	7
159	Laboratory ultrasonic measurements: Shear transducers for compressional waves. The Leading Edge, 2019, 38, 392-399.	0.7	7
160	A Laboratory Forced-Oscillation Apparatus for Measurements of Elastic and Anelastic Properties of Rocks at Seismic Frequencies. Frontiers in Earth Science, 2021, 9, .	1.8	7
161	Fluid–Fluid Interfacial Effects in Multiphase Flow during Carbonated Waterflooding in Sandstone: Application of X-ray Microcomputed Tomography and Molecular Dynamics. ACS Applied Materials & Interfaces, 2021, 13, 5731-5740.	8.0	7
162	A New Approach To Calculate Gas Saturation in Shale Reservoirs. Energy & Fuels, 2022, 36, 1904-1915.	5.1	7

#	Article	IF	CITATIONS
163	Heterogeneities in the elastic properties of microporous carbonate rocks at the microscale from nanoindentation tests. , 2015, , .		6
164	On the interpretation of ultrasonic laboratory measurements in anisotropic media. Geophysics, 2018, 83, C173-C178.	2.6	6
165	Elastic properties of sands, Part 1: Micro computed tomography image analysis of grain shapes and their relationship with microstructure. Geophysical Prospecting, 2019, 67, 723-744.	1.9	6
166	The effect of wave amplitude on S-wave velocity in porous media: an experimental study by Laser Doppler Interferometry. Exploration Geophysics, 2019, 50, 683-691.	1.1	6
167	Xâ€ray microâ€computed tomography analysis of accumulated corrosion products in deepâ€water shipwrecks. Materials and Corrosion - Werkstoffe Und Korrosion, 2019, 70, 1977-1998.	1.5	6
168	Elastic Moduli of Arenites From Microtomographic Images: A Practical Digital Rock Physics Workflow. Journal of Geophysical Research: Solid Earth, 2020, 125, e2020JB020422.	3.4	6
169	In Situ Wettability Investigation of Aging of Sandstone Surface in Alkane via X-ray Microtomography. Energies, 2020, 13, 5594.	3.1	6
170	Investigating the mechanism of microbiologically influenced corrosion of carbon steel using X-ray micro-computed tomography. Journal of Materials Science, 2021, 56, 13337-13371.	3.7	6
171	Experimental Study on Petrophysical Properties as a Tool to Identify Pore Fluids in Tight-Rock Reservoirs. Frontiers in Earth Science, 2021, 9, .	1.8	6
172	Effect of pore fluid on ultrasonic S-wave attenuation in partially saturated tight rocks. International Journal of Rock Mechanics and Minings Sciences, 2021, 147, 104910.	5.8	6
173	Mechanical and Electrical Properties of Al2O3 Thin Films on Metals, Ceramics and Resins Prepared by Aerosol Deposition Method. Ceramic Engineering and Science Proceedings, 0, , 121-125.	0.1	6
174	A Low-frequency Apparatus for Characterizing the Mechanical Properties of Rocks. , 2011, , .		6
175	Supersonic heat wave in low density foams generated by soft X-radiation from a Z-pinch plasma. Physics Letters, Section A: General, Atomic and Solid State Physics, 1998, 240, 73-76.	2.1	5
176	Laboratory measurements of ultrasonic velocities in CO2 saturated brines. Energy Procedia, 2014, 63, 4273-4280.	1.8	5
177	Wave attenuation in partially saturated porous rocks — New observations and interpretations across scales. The Leading Edge, 2014, 33, 606-614.	0.7	5
178	A laboratory study of the elastic anisotropy in the Mancos Shale at seismic frequencies. , 2016, , .		5
179	Experimental Study of Supercritical CO2 Injected into Water Saturated Medium Rank Coal by X-ray MicroCT. Energy Procedia, 2018, 154, 131-138.	1.8	5
180	A Realistic Look at Nanostructured Material as an Innovative Approach for Enhanced Oil Recovery Process Upgrading. , 2018, , .		5

#	Article	IF	CITATIONS
181	Elastic properties of a reservoir sandstone: a broadband interâ€ŀaboratory benchmarking exercise. Geophysical Prospecting, 2021, 69, 404-418.	1.9	5
182	Wettability of Shale/Oil/Brine Systems: A New Physicochemical and Imaging Approach. , 2022, , .		5
183	PZT-Driven Micromagnetic Optical Devices. Materials Research Society Symposia Proceedings, 2003, 785, 6101.	0.1	4
184	A Seismicâ€Frequency Laboratory Study of Solid Substitution in Bentheim Sandstone. Journal of Geophysical Research: Solid Earth, 2019, 124, 5492-5499.	3.4	4
185	Elastic properties of sands, Part 2: Implementation of contactâ€based model to determine the elasticity of the grains from ultrasonic measurements. Geophysical Prospecting, 2019, 67, 745-760.	1.9	4
186	Estimation of Carbonate Elastic Properties Using Nanoindentation and Digital Images. , 2010, , .		4
187	Changes in Microstructure and Elastic Properties of Mancos Shale after Pyrolysis. , 2014, , .		4
188	Fracturing of organic-rich shale during heating. , 2013, , .		3
189	An Experimental Study of Low-Frequency Wave Dispersion and Attenuation in Water Saturated Sandstones. , 2013, , .		3
190	Laboratory measurements of the elastic and anelastic parameters of limestone at seismic frequencies. , 2013, , .		3
191	Effect of pyrolysis on elastic properties and microstructure of organic-rich Mancos shale. , 2014, , .		3
192	Changes in microstructure and mineralogy of organic-rich shales caused by heating. ASEG Extended Abstracts, 2015, 2015, 1-4.	0.1	3
193	CO2 saturated brine injected into fractured shale: An X-ray micro-tomography in-situ analysis at reservoir conditions. Energy Procedia, 2018, 154, 125-130.	1.8	3
194	Estimation of grain elasticity properties from ultrasonic measurements on dry granular pack. Geophysical Prospecting, 2018, 66, 1726-1736.	1.9	3
195	A solid/fluid substitution scheme constrained by pore-scale numerical simulations. Geophysical Journal International, 2020, 220, 1804-1812.	2.4	3
196	A novel approach to determine the Biot's coefficient using X-ray computed tomography. Bulletin of Engineering Geology and the Environment, 2021, 80, 7865-7877.	3.5	3
197	Laboratory measurements with DAS: A fast and sensitive tool to obtain elastic properties at seismic frequencies. The Leading Edge, 2021, 40, 655-661.	0.7	3
198	The Effect of Constriction in Hydraulic Fracturing. Springer Series in Geomechanics and Geoengineering, 2017, , 613-619.	0.1	3

#	Article	IF	CITATIONS
199	A Laboratory Study of the Effect of Boundary Conditions on the Elastic Moduli Measurements. , 2019, ,		3
200	P-wave scattering by randomly distributed aligned cracks in fractal media. Geophysical Journal International, 0, , .	2.4	3
201	Simultaneous experimental study of dynamic and static Young's moduli in sandstones. Exploration Geophysics, 2021, 52, 601-611.	1.1	3
202	Optical micro-scanner fabricated on stainless steel by aerosol deposition method. , 0, , .		2
203	Direct laboratory observation of velocityâ€saturation relation transition during rocks saturation. , 2008, , .		2
204	Ultrasonic measurements of S waves using laser interferometry. , 2014, , .		2
205	Elastic anisotropy of the Wellington shale at seismic frequencies: Laboratory measurements. , 2016, , .		2
206	Ultrasonic characterization of anisotropic rocks: Impact of transducers' size and geometry on data interpretation. Geophysics, 2020, 85, C99-C105.	2.6	2
207	Bulk moduli of sandstones subjected to isotropic stress: Simultaneous static and dynamic experimental study. Journal of Applied Geophysics, 2021, 191, 104344.	2.1	2
208	Laboratory study of the influence of changing the injection rate on P-wave velocities and water saturation in a Limestone. ASEG Extended Abstracts, 2012, 2012, 1-4.	0.1	2
209	Low-frequency measurements of the mechanical parameters of sandstone with low permeability. ASEG Extended Abstracts, 2012, 2012, 1-4.	0.1	2
210	A Laboratory Study of Elastic and Anelastic Properties of Savonnieres Limestone. , 2014, , .		2
211	The Influence of CO2 Saturated Brine on Microstructure of Coal: Implications for Carbon Geo-Sequestration. Frontiers in Energy Research, 2022, 10, .	2.3	2
212	The dead volume effect on the elastic moduli measurements using the forcedâ€oscillation method. Geophysical Prospecting, 2022, 70, 547-557.	1.9	2
213	Dynamic properties of PZT thick films structured on Si membrane by the aerosol deposition method. , $0,$, .		1
214	Thick PZT film/stainless steel actuator fabricated by aerosol deposition method: fatigue property. , 2002, 4936, 345.		1
215	Optical scanning devices based on PZT thick films formed by aerosol deposition method. , 2005, 6037, 474.		1
216	Comments on "Electrical conductivity of open-cell metal foams―by K.P. Dharmasena and H.N.G. Wadley [J. Mater. Res. 17, 625 (2002)]. Journal of Materials Research, 2008, 23, 1202-1206.	2.6	1

#	Article	IF	CITATIONS
217	Softening of rocks matrix due to water flood: Experimental study. , 2014, , .		1
218	Stress-dependence of elastic properties of rock containing finite cracks with contacting surfaces. , 2015, , .		1
219	Joint inversion of P-, and S-wave travel times for characterisation of anisotropic materials using laser Doppler interferometry measurements. ASEG Extended Abstracts, 2015, 2015, 1-4.	0.1	1
220	Acoustics of Partially Saturated Rocks: Theory and Experiments. , 2015, , 45-75.		1
221	Inverting Dynamic Elastic Moduli of a Granular Pack to Get Shear Modulus of the Grain. ASEG Extended Abstracts, 2016, 2016, 1-5.	0.1	1
222	Seismic Effects of Viscoelastic Pore Fill on Double-Porosity Rocks. , 2017, , .		1
223	Prediction of Hydrate Phase Equilibrium Conditions for Different Gas Mixtures. , 2018, , .		1
224	Reactive Flow in Unconsolidated Sandstone: Application to Carbon Geosequestration. , 2018, , .		1
225	Pore Scale Analysis the Formation Dissolution with Capillary Trapping Change for CO2 Injected into Carbonate Reservoir. , 2018, , .		1
226	Acoustic properties of rocks compacted from powders ASEG Extended Abstracts, 2015, 2015, 1-4.	0.1	1
227	Low Frequency Measurements of the Elastic and Anelastic Properties of the Sandstone Flooded with Supercritical CO2. , 2013, , .		1
228	Computation of Elastic Properties Based on Microtomogram Images. , 2011, , .		1
229	Effect of Grain Shapes in Coordination Number from Micro-CT Image Analysis of an Unconsolidated Sand. , 2017, , .		1
230	Ultrasonic Velocities of Unconsolidated Sand: Evaluating the Microstructure and Contact Based Models. , 2017, , .		1
231	An Optimized Digital Rock Physics Workflow for Elastic Moduli Estimation of Sandstones with Dispersed Clay. , 2020, , .		1
232	Excitation of intense shock waves by soft X-radiation from a Z-pinch plasma. AIP Conference Proceedings, 1996, , .	0.4	0
233	Generation of shock waves by soft x-radiation from z-pinch plasma. AIP Conference Proceedings, 1996, ,	0.4	0
234	Fabrication of microfluidic devise (diffuser or mixer) using aerosol deposition method. , 2002, , .		0

#	Article	IF	CITATIONS
235	Practical High-Speed Metal-Based Optical Microscanning Devices with Low Production Cost. , 0, , .		0
236	11. Poroelasticity. , 2010, , 235-254.		0
237	Estimation of Carbonate Elastic Properties from Nanoindentation Experiments to Reduce Uncertainties in Reservoir Modelling. ASEG Extended Abstracts, 2010, 2010, 1-4.	0.1	Ο
238	Laboratory measurements of seismic velocities of CO2/brine mixtures at elevated temperatures up to 70°C and pressures up to 38 MPa. ASEG Extended Abstracts, 2013, 2013, 1-4.	0.1	0
239	Experimental laboratory study on the acoustic response during injection of supercritical CO2 into brine saturated sandstones. ASEG Extended Abstracts, 2013, 2013, 1-4.	0.1	Ο
240	Low-frequency laboratory measurements of the acoustic parameters of Savonnieres limestone. , 2014, , ,		0
241	Changes in elastic properties of artificial shales due to compaction. ASEG Extended Abstracts, 2015, 2015, 1-4.	0.1	0
242	True-Triaxial-cell set up to estimate the stress induced anisotropy: Uniformity study. ASEG Extended Abstracts, 2016, 2016, 1-4.	0.1	0
243	Ultrasonic measurements on thin samples: numerical modelling. ASEG Extended Abstracts, 2016, 2016, 1-5.	0.1	Ο
244	Ultrasonic measurements on thin samples: Experiment and numerical modeling. , 2016, , .		0
245	A two-scale geostatistical approach for elastic properties estimation. , 2017, , .		0
246	Compaction Trends of Permeability in Artificial Shales Measured Using Pressure-oscillation Technique. , 2017, , .		0
247	Optimum Image Resolution of a micro-CT image to characterize shape descriptors of unconsolidated sand. ASEG Extended Abstracts, 2018, 2018, 1-8.	0.1	0
248	The impact of water saturation on the elastic anisotropy dispersion in the Wellington shale at seismic frequencies. ASEC Extended Abstracts, 2018, 2018, 1-5.	0.1	0
249	Coupled measurements of hydraulic permeability and full stiffness tensor compaction trends in artificial shales. ASEG Extended Abstracts, 2018, 2018, 1-7.	0.1	Ο
250	Experimental and Theoretical Study of Water Retention Effects on Elastic Properties of Opalinus Shale. ASEG Extended Abstracts, 2018, 2018, 1-8.	0.1	0
251	Effect of Amplitude on Wave Propagation. ASEG Extended Abstracts, 2018, 2018, 1-5.	0.1	0
252	The Elastic Moduli Change After Carbon Dioxide Flooding Into Limestone: An Experimental Study. ,		0

2018,,.

MAXIM LEBEDEV

#	Article	IF	CITATIONS
253	Forward and inversion modelling of the ultrasonic wave in a homogeneous medium using P-wave transducers. ASEG Extended Abstracts, 2018, 2018, 1-7.	0.1	0
254	Estimation of elastic anisotropy from three-component ultrasonic measurements using laser Doppler interferometry. Exploration Geophysics, 2018, 49, 744-750.	1.1	0
255	Assessing mineral composition and permeability of a shale seal. ASEG Extended Abstracts, 2019, 2019, 1-5.	0.1	0
256	The effects of stress and fluid on the anisotropy of reservoir rock: case study of a sandstone from the harvey 3 CCS site, Western Australia. Exploration Geophysics, 2020, 51, 434-445.	1.1	0
257	Highâ€Precision Tracking of Sandstone Deformation From Microâ€CT Images. Journal of Geophysical Research: Solid Earth, 2021, 126, e2021JB022283.	3.4	0
258	CO2 laser annealing of Pb(Zr,Ti)O3 aerosol-deposition film on stainless-steel-sheet. , 2005, , 249-252.		0
259	Finite-difference Numerical Experiments and Laboratory Testing of Attenuation and Dispersion in Patchy-saturated Media. , 2009, , .		0
260	Experimental Estimation of Compressional Velocities of a Series of Swedish Crystalline Rocks and Ores. , 2011, , .		0
261	An Experimental Study of Low-frequency Wave Dispersion and Attenuation in Water Saturated Sandstone. , 2012, , .		0
262	Elastic Properties of Lochaline Sandstone - Numerical Experiment vs. Measurements. , 2012, , .		0
263	3C laboratory measurement using laser interferometer. ASEG Extended Abstracts, 2012, 2012, 1-4.	0.1	0
264	Low frequency laboratory measurements of the elastic and anelastic properties of the sandstone flooded with supercritical CO2. ASEG Extended Abstracts, 2013, 2013, 1-4.	0.1	0
265	An experimental study of modulus dispersion and attenuation in sandstones at seismic frequencies. ASEG Extended Abstracts, 2013, 2013, 1-4.	0.1	0
266	A laboratory study of the "barrel shape―effect in a viscoelastic cylindrical sample at seismic frequencies. ASEG Extended Abstracts, 2015, 2015, 1-2.	0.1	0
267	Generalized squirt theory for an arbitrary viscoelastic pore fill and partial saturation. , 2016, , .		0
268	The coupling of elastic properties and hydraulic permeability in artificial shales. , 2017, , .		0
269	3D pore scale analysis of limestone matrix dissolution in CO2 EOR and geosequestration. , 2017, , .		0
270	The overestimated elastic moduli from digital rock images: Computational reasons. , 2020, , .		0